J. Phys. B: At. Mol. Opt. Phys. **33** (2000) 5215–5224. Printed in the UK PII: S0953-4075(00)51256-5

Emission cross sections for H, C and He produced in $He^+ + CH_4$ collisions

Kenji Motohashi† and Seiji Tsurubuchi

Department of Applied Physics, Tokyo University of Agriculture and Technology, 2-24-16 Koganei, Tokyo 184-8588, Japan

E-mail: motohasi@cc.tuat.ac.jp

Received 7 July 2000, in final form 2 October 2000

Abstract. Emission cross sections for hydrogen Lyman-α, -β, Balmer-α, -β, C($3s\ ^3P^o_{J'} \rightarrow 2p^2\ ^3P_J$, 165.7 nm), C($2p^3\ ^3D^o_{J'} \rightarrow 2p^2\ ^3P_J$, 156.1 nm) and He($2p\ ^1P_1 \rightarrow 1s^2\ ^1S_0$, 58.4 nm) produced in $He^+ + CH_4$ collisions are measured in the energy range from 4 eV (cm) to 4000 eV (cm). The emission cross sections of hydrogen Lyman and Balmer series have a plateau above 100 eV. The cross sections of helium and carbon lines decrease rapidly with decreasing collision energy. The branching ratio when an excited hydrogen with $n = 2$ is produced is estimated to be 2.5×10^{-2} at 4000 eV by using measured emission cross sections for H_α to H_ε and by empirical relations.

1. Introduction

Charge exchange in $He^+ + CH_4$ collisions is an important process that is frequently seen in fusion plasmas. Knowledge of the optical emission cross sections of this system is important for diagnosis in tokamak devices. The reaction of $He^+ + CH_4$ is also quite important in the chemistry of the ionosphere of the outer planets as He^+ ions and CH_4 are both present in significant concentrations [1]. The rate coefficient for $He^+ + CH_4$ is larger than that for $He^+ + H_2$ by 1.5×10^4 [2]. However, there are only a few reports on the cross sections for this collision system. No papers, to the authors' knowledge, have reported on the emission cross sections for fragments split from CH_4 in the energy range from a few eV to several keV.

Bryan *et al* [3] measured the Balmer-α emission cross sections produced by collision of 100–350 keV He^+ incident on H_2, CH_4, C_2H_2, C_2H_4 and C_2H_6. They found that the Bethe–Born approximation is valid in these collision systems in that energy range, and found that the Bragg additivity rule is not applicable at these energies. Tsuji *et al* [4] studied dissociative excitation of CH_4 in collisions with He($2\ ^3S$), He^+ and He^{2+} by observing CH($A\ ^2\Delta$–$X\ ^2\Pi$, $B\ ^2\Sigma^-$–$X\ ^2\Pi$ and $C\ ^2\Sigma^+$–$X\ ^2\Pi$) and Balmer-α emissions in a flowing afterglow experiment. They obtained emission rate coefficients and emission cross sections of their spectra in the case of an He($2\ ^3S$) + CH_4 reaction at near thermal energy and determined the rotational and vibrational temperatures of CH($A\ ^2\Delta$) and CH($B\ ^2\Sigma^-$) by fitting experimental band intensities to calculated ones. They found that the CH(A–X, B–X and C–X) band and Balmer emissions produced in the collision of He($2\ ^3S$) were not reduced by adding SF_6, while the band emissions produced by He^+ and He^{2+} collisions were completely suppressed. They

† Author to whom correspondence should be addressed.

0953-4075/00/225215+10$30.00

also found no significant change in intensities for the band and for the Balmer emissions when He^+ and He^{2+} were trapped by an ion-collector grid. They concluded that CH^*(A, B, C) and $H^*(n = 3$ and 4) are not produced in $He^+ + CH_4$ collisions at near thermal energy.

There are several works which report detecting fragment ions produced in $He^+ + CH_4$ collisions. Most measurements are performed at a thermal or MeV energy range. Adams and Smith [5] observed ionized-product distributions for the reactions of He^+ ions with N_2, O_2, CO_2 and CH_4, and N^+ ions with O_2 by the SIFT (selected ion flow tube) technique. They reported that the ions H_2^+, H_3^+, HeH^+ and C^+ were not observed experimentally and concluded that CH_n^+ ($n = 0$–4) ions are produced via a direct charge transfer to produce highly excited CH_4^+ but not via an intermediate complex because of the absence of HeH^+. Huntress *et al* [6] and Kim and Huntress [7] also reported ionized-product distributions for reactions of the He^+ ion with CH_4 with thermal energy. Catham *et al* [8] measured the rate coefficients for the reactions of He^+, Ne^+ and Ar^+ with CH_4, C_2H_6, SiH_4 and Si_2H_6, and compared them with the Langevin values. The He^+ rate coefficient of CH_4 was reported to be about half of the Langevin value. They observed C^+ ions above $E_{cm} \sim 0.1$ eV. There is good agreement on the product ion distribution among these experiments. Bowers and Elleman [9] measured charge transfer rate constants from He^+, Ne^+, Ar^+, Kr^+ and Xe^+ to CH_4, CD_4, C_2H_6, C_3H_8 and SiH_4 using ion cyclotron resonance spectroscopy. Varghese *et al* [10] and Itoh *et al* [11] measured single- and/or double-electron capture cross sections for He^+ and carbon-containing molecules including CH_4 collisions in the 0.7–3.2 MeV region. Total charge exchange cross sections or secondary ion formation cross sections were reported by Koopman [12] and Browning *et al* [13] below 1.4 keV and below 45 keV, respectively.

The $(2a_1)^{-1}$ ionic states of CH_4 were found to be 22.4 eV by photoabsorption and by electron energy loss experiments [14, 15]. Several $(2a_1)^{-1}n\ell$ Rydberg states with a C–H symmetric stretch converging to the $(2a_1)^{-1}$ state were found to be around 19–23 eV [16]. We had concluded in our previous work with electron impact measurements [17] that the Lyman and Balmer emissions of the hydrogen atom produced by electron impact on CH_4 were mainly caused by the dissociation process of $H^*(n\ell) + CH_3$ via $2a_1 \rightarrow n\ell$ superexcitation. From an energy point of view, however, the possibility of $H^*(n\ell)$ formation by $H^*(n\ell) + CH_3^+$ via $(2a_1)^{-1}$ cannot be excluded. If the potential energy of 24.6 eV produced by the charge exchange process is transferred to CH_4, it is possible that $H^*(n\ell)$ is produced by these dissociation processes. We have measured optical emission cross sections for the fragment species produced in the $He^+ + CH_4$ reaction with impact energy as low as 4 eV to verify this possibility.

2. Experiment

A schematic of the experimental set-up is presented in figure 1. The apparatus consists of a collision chamber, an ion source, a mass-analysing magnet, a VUV monochromator and a visible monochromator. The collision chamber has a diameter of 40 cm. The residual gas pressure is kept below 2.6×10^{-5} Pa by a turbo-molecular pump. CH_4 gas (99.999%) is continuously introduced from the bottom of the chamber through a variable leak valve. The pressure of CH_4 gas is typically 1.3×10^{-2} Pa, which is measured by an ionization gauge calibrated by a capacitance manometer. All measurements are performed under the condition that the emission intensity is always proportional to both the ion current and the target pressure to ensure a single collision between an ion and a molecule.

The ion source is a conventional duoplasmatron type with a permanent magnet. The He^+ beam current, which is extracted by 3.0 kV, is typically 0.5 μA after mass analysis with

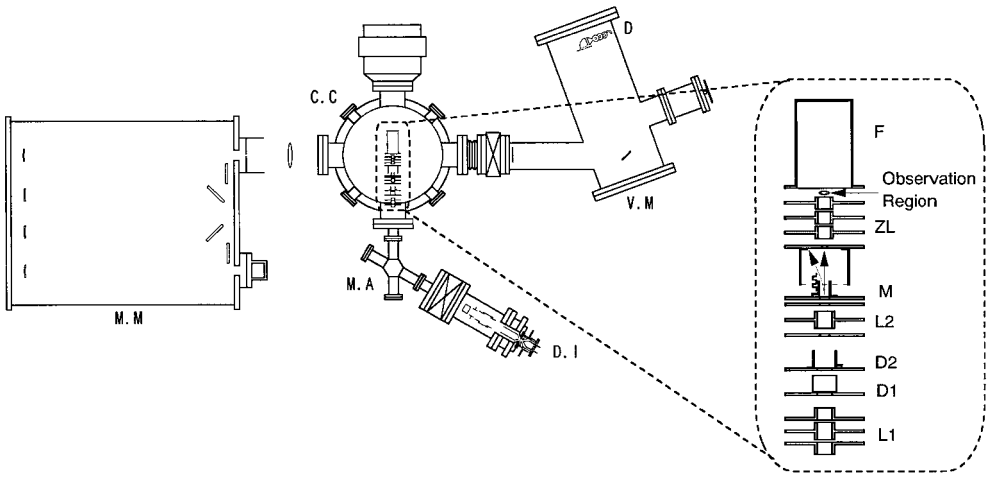

Figure 1. Schematic of the experimental apparatus. MM, visible monochromator; MA, mass-analysing magnet; DI, duoplasmatron ion source; CC, collision chamber; VM, vacuum monochromator (Seya–Namioka VUV monochromator); D, detector (channel electron multiplier); L1, L2, einzel lenses; D1, vertical deflector; D2, horizontal deflector; M, beam modulator; ZL, zoom lens; F, Faraday cup.

a 60°-type sector magnet. The beam line after the analysing magnet is also illustrated in figure 1. It consists of two pairs of einzel lenses, a pair of deflectors for steering, a deflector for modulation, a deceleration lens and a Faraday cup. The space between the Faraday cup and the third electrode of the deceleration lens forms an observation region that is biased to the deceleration voltage through an optical coupler. The ion beam current is detected by means of current-to-frequency and frequency-to-voltage conversions. The ion current of 0–1 μA is converted to the pulse sequence of 0–10 kHz. A Seya–Namioka-type VUV monochromator with a grating of 1200 grooves/mm blazed at 120 nm and a visible double monochromator with two gratings of 1200 grooves/mm blazed at 500 nm are set facing opposite directions as shown in figure 1. The angle between the ion beam axis and the optical axis is 90°. The visible emission is detected by a photomultiplier, while the VUV emission is detected by a channel electron multiplier with a CsI-coated CuBeO photocathode. A synchronous single-photon counting technique with a modulated ion beam is used to detect weak signals. The optical quantum efficiency $k(\lambda)$ in the visible wavelength region is determined by a standard light source (400–800 nm) and a deuterium lamp (250–400 nm). The efficiency curve obtained is carefully checked by measuring well established emission cross sections for He given by Van Zyl *et al* [18]. The relative quantum efficiency in the VUV region is determined by comparing intensities of various spectra produced in $e^- + H_2$, $e^- + Ar$ and $e^- + He$ with their calibrated intensities or cross sections [15–17]. An absolute emission cross section for H_α produced by He^+ impact on H_2 ($E_{cm} = 2400$ eV) is obtained by comparing spectral intensities with the intensity of Ar I ($4p'\left[\frac{1}{2}\right]_0 \rightarrow 4s'\left[\frac{1}{2}\right]^o_1$: 750.4 nm) produced by the electron impact of Ar whose absolute cross section ($(2.21 \pm 0.24) \times 10^{-18}$ cm^2) at 100 eV is previously determined in our laboratory by an absolute measurement [19]. In the normalization procedure, the lens electrode system was removed and an electron gun was placed at the collision region so that the electron beam axis coincides with the ion beam axis.

An absolute emission cross section for hydrogen Lyα, $(3.4 \pm 1.4) \times 10^{-17}$ cm^2, produced by He^+ impact on H_2 ($E_{cm} = 2400$ eV) given by Van Zyl *et al* [20] is used as a standard cross

section in the VUV wavelength region. The possibility that some fast fragments escape from the focal point during the residence time is considered small for the following reasons. The fastest fragment observed in the present experiment is He(2 ^{1}P) accelerated by 4000 eV. The velocity of this He(2 ^{1}P) is about 4.4×10^5 m s^{-1}, and the residence time is about 23 ns for the observation region of 10 mm. Intensity attenuation of He(2p ^{1}P $\rightarrow$ 1s ^{1}S: 58.4 nm) is calculated to be 2.2×10^{-18} by taking into account the lifetime of 0.56 ns. This attenuation of the emission is negligible. The Lyα cross sections obtained by the method described here are carefully checked by another method as discussed in the next section. The collision energy is determined by scanning the retarding bias potential. We define the zero-energy point as the maximum position of the derivative curve of the ion current versus the retarding bias. The energy resolution defined by the full width at half maximum of the derivative curve is 9 eV.

3. Results and discussion

As described in section 2, cross section measurements must be taken under conditions such that the emission intensities are proportional to both the ion beam current and the target gas pressure. We checked the linearities for H(Lyα), C(156.1 nm) and He(58.4 nm) transitions at 20, 100 and 3000 eV in the laboratory frame. The pressure dependence of normalized emission intensities of H(Lyα) and C(156.1 nm) are shown in figure 2. Linearity breaks down above 4.1×10^{-2} Pa for H(Lyα) and 2.9×10^{-2} Pa for C(165.7 nm), respectively. Therefore, cross section measurements were carried out under a target pressure of below 1.3×10^{-2} Pa. Absolute cross sections of VUV emission at 2400 eV (cm) were determined by normalizing the intensity of each spectrum to that of the H(Lyα) produced in $He^+ + H_2$ [20]. The cross section of hydrogen Lyα produced in $He^+ + CH_4$ determined by this normalization is $(7.5 \pm 3.1) \times 10^{-17}$ cm^2. The H(Lyα) cross section determined by normalizing the relative intensity to that of $H^+ + Ar$ as reported by Pretzer *et al* [21] is $(7.4 \pm 2.5) \times 10^{-17}$ cm^2. Excellent agreement is found between the two values obtained by different normalization procedures, which indicates that

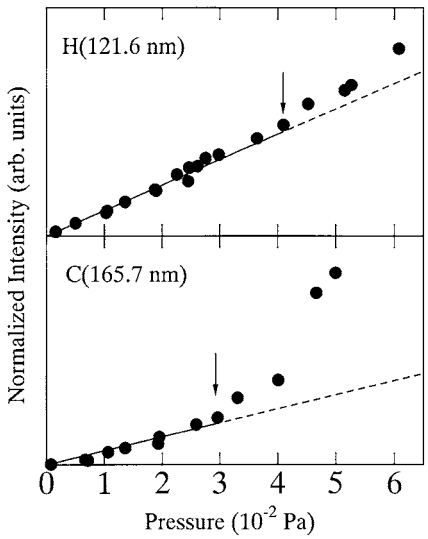

Figure 2. Pressure dependence of the normalized emission intensities in H(121.6 nm) and C(165.7 nm). The arrows indicate the pressure at which linearity breaks down.

Table 1. Emission cross sections of hydrogen, carbon and helium transitions produced in $He^+ + CH_4$ at 2400 eV (cm).

Species	σ (10^{-18} cm^2)
H(Lyα)	75 ± 31
H(Lyβ)	13.0 ± 4.8
H_α	21.3 ± 3.8
H_β	3.7 ± 1.1
C(156.1 nm)	2.9 ± 0.9
C(165.7 nm)	3.5 ± 1.5
He(58.4 nm)	2.3 ± 1.1

the cross section has little systematic error. Absolute cross sections of visible emissions at 2400 eV (cm) are determined by comparing intensities of each spectrum with that of Ar I ($4p'\left[\frac{1}{2}\right]_0 \rightarrow 4s'\left[\frac{1}{2}\right]^o_1$, 750.3 nm) produced by electron impact of Ar [19]. The H_α emission cross section obtained by this normalization is $(2.13 \pm 0.38) \times 10^{-17}$ cm^2.

The emission cross sections at 2400 eV (cm) of all fragments observed in the present experiment are listed in table 1. It should be noted that the cross section for He (58.4 nm) produced in the process

$$He^+ + CH_4 \rightarrow He(2\ ^1P) + CH_4^+ - 9.2\ \text{eV} \tag{1}$$

is quite large despite having the largest energy defect (ΔE_∞) among all processes, which suggests that charge exchange plays an important role in the dissociation process. Emission cross sections as a function of collision energy are shown in figures 3(*a*)–(*d*). In the case of hydrogen spectra, all cross sections show a similar energy dependence, having a plateau above 100 eV. Although the position of the first onset is not clear, extrapolating from the data in the figures, it seems to be at a few eV. The carbon spectra also have a similar energy dependence which increases monotonically with increasing energy. Large uncertainties are included in their cross sections because of a poor signal-to-noise ratio caused by small quantum efficiencies. We cannot say at this stage whether their cross sections have a threshold or not. Due to large statistical errors, it is also difficult to say whether the emission cross section for the 58.4 nm line of He has any significant structure like both carbon transitions.

Cross section data which can be compared with the present results have not yet been reported. Bryan *et al* [3] measured the emission cross section of hydrogen Balmer-α from collisions of He^+ on H_2, CH_4, C_2H_2, C_2H_4 and C_2H_6 in the energy range from 100 to 350 keV. Their cross section maximum is observed at 37.5 keV u^{-1} (lab). Roughly speaking, their cross section value ($(2.20–3.61) \times 10^{-17}$ cm^2) agrees with the order of magnitude of the present data. Tsuji *et al* [4] concluded that $H^*(n = 3, 4)$ are not produced by the reaction of $He^+ + CH_4$ in the flowing afterglow. This is due to the collision energy being lower than the dissociation energy limit. The average collision energy calculated using the previous results published by the same group [22] is about 0.045 eV, whereas the energy defects are 1.8 and 2.5 eV in these endothermic processes.

The lowest dissociation channels producing H(2p), C(3s $^3P^o_{J'}$) and C(2p^3 $^3D^o_J$) are as follows:

$$He^+ + CH_4 \rightarrow He + CH_3^+ + H(2p) + 0.1\ \text{eV} \tag{2}$$

$$He^+ + CH_4 \rightarrow He + H_2 + H_2^+ + C(3s\ ^3P^o_J) - 6.6\ \text{eV} \tag{3}$$

and

$$He^+ + CH_4 \rightarrow He + H_2 + H_2^+ + C(2p\ ^3D^o_J) - 7.1\ \text{eV}. \tag{4}$$

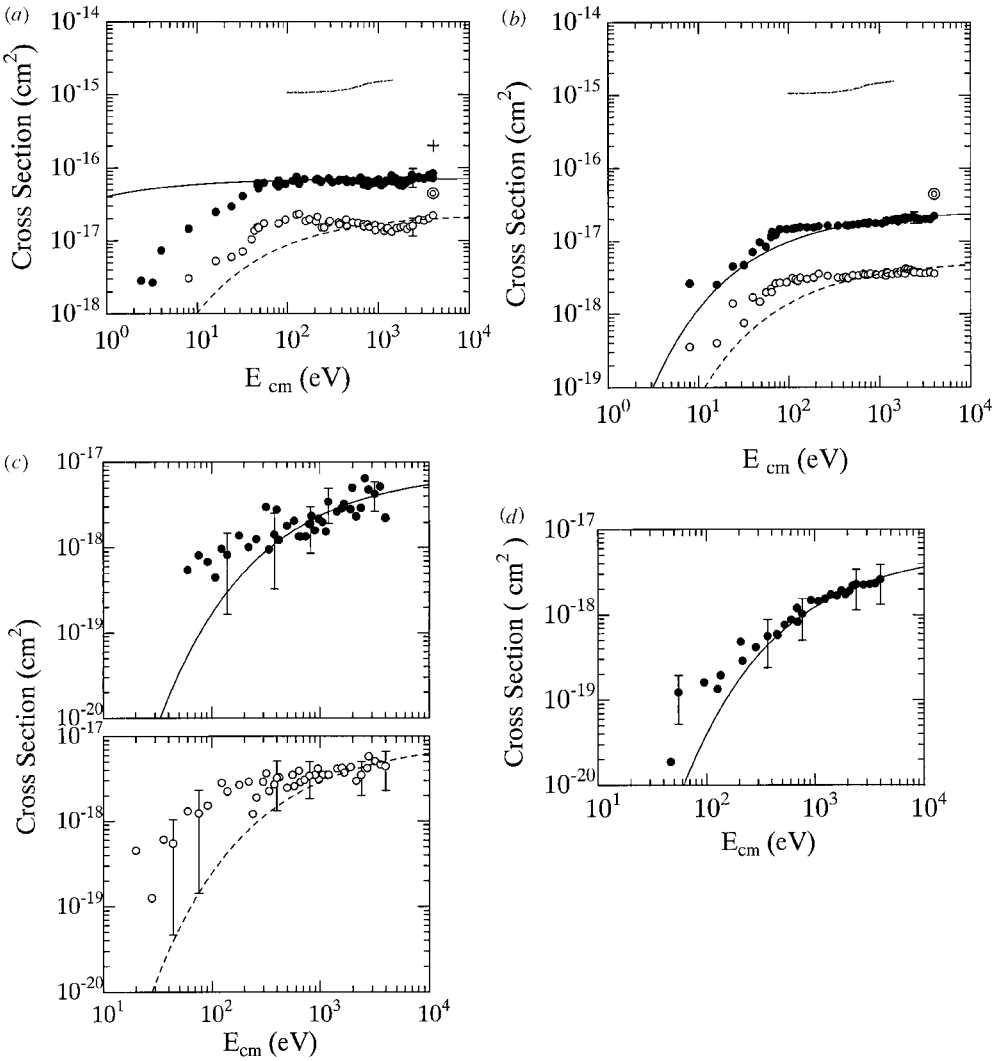

Figure 3. (*a*) Emission cross sections of the present results for Lyα (●) and Lyβ (○). The cross sections for producing excited hydrogen in $n = 2$ and 3 in process (2) are also displayed as a cross and a double circle, respectively. Full and broken curves show the semiquantitative theory of Lyα and Lyβ cross sections calculated by equations (6) and (7). Both curves are normalized to the experimental data at 4000 eV. — · —, total charge-exchange cross section (Koopman [12]). (*b*) Emission cross sections of the present results for H_α (●) and H_β (○). The cross sections for producing excited hydrogen in $n = 3$ in process (2) are also displayed as a double circle. ——, H_α cross section calculated by equations (6) and (7). – – –, H_β cross section calculated by equations (6) and (7). Both curves are normalized to the experimental data at 4000 eV. — · —, total charge-exchange cross section (Koopman [12]). (*c*) ●, C(156.1 nm), ○, C(165.7 nm). ——, cross section of C(156.1 nm) calculated by equations (6) and (7). – – –, cross section of C(165.7 nm) calculated by equations (6) and (7). Both curves are normalized to the experimental data at 4000 eV. (*d*) ●, cross section for the resonance line (58.4 nm) of He. ——, cross section of He(58.4 nm) calculated by equations (6) and (7). This curve is normalized to the experimental data at 4000 eV.

Though only H(2p) production process (2) is exothermic, its cross section decreases with decreasing energy. Therefore, the kinetic energy of a few eV may be distributed to CH_3^+ and H. Because all hydrogen cross sections have a similar energy dependence, it is concluded that CH_4^{+*} producing $CH_3^+ + H^*(n)$ forms a Rydberg-like state. All dissociative excitation processes except for process (2) are endothermic. The energy defects producing $H(3\ell)$ and $H(4\ell)$ also have slight negative values. The cross section tends to have a larger value with a decreasing energy defect at a low collision energy. The order of the cross section below 100 eV,

$$\sigma_H(\mathrm{Ly}\alpha) > \sigma_H(\mathrm{Ly}\beta) \sim \sigma_H(\mathrm{H}_\alpha) > \sigma_H(\mathrm{H}_\beta)$$
$$> \sigma_C(156.1\ \mathrm{nm}) \sim \sigma_C(165.7\ \mathrm{nm}) > \sigma_{He}(58.4\ \mathrm{nm}) \tag{5}$$

coincides with that of exothermicity. According to the semiquantitative theory of Massey and Burhop [23], the maximum cross section for non-resonant charge exchange should occur for the collision velocity

$$v_m = a|\Delta E_\infty|/h \tag{6}$$

and in the velocity region below v_m, the cross section should have the form

$$\sigma \propto \exp(-a|\Delta E_\infty|/4hv) \tag{7}$$

where a is a length determined empirically to be about 0.7–0.8 nm in typical cases [24, 25] and h is Planck's constant. By substituting each value of $|\Delta E_\infty|$ specified in equations (1)–(4) and $a = 0.7$ nm into equations (6) and (7), we obtain the results shown in figures 3(*a*)–(*d*). The calculated results are in good agreement with experimental results above 400 eV, though, except for the Lyα emission, they underestimate in the energy region below 400 eV. One of the possible reasons for the underestimation in the low-energy region is the increased probability of formation of the $(HeCH_4)^{+*}$ quasimolecule. On the other hand, the overestimation of the Lyα cross section under 40 eV may be due to energy loss from nuclear motion of rotational and/or vibrational excitations. We hypothesize that the second onset of Lyβ around ~ 1500 eV is due to the following processes:

$$He^+ + CH_4 \rightarrow He + CH_2^+ + H_2 + H(3) - |\Delta E_\infty| \tag{8}$$

where $|\Delta E_\infty|$ is 7.2 eV. The cross section should have a maximum value at a collision velocity of 1.2×10^6 m s^{-1}, which corresponds to a collision energy of 31 keV. The tendency for the cross section to decrease with increasing $|\Delta E_\infty|$ as observed in this paper is consistent with equation (7). Knowledge of the potential surfaces is necessary for further discussion.

In addition, we discuss the relationship between the total charge-transfer cross section and the present results. The total charge-exchange cross section [12] is nearly flat below a slight onset around 400 eV, whereas the excitation functions in the present results decrease rapidly as the collision energy decreases below several hundred eV. We suggest that the onset around 400 eV as reported by Koopman [12] is caused by the excited species. In other words, neutral and ionic species in the ground state contribute to the part of the cross sections which is almost flat as a function of the collision energy.

Finally, we estimate the branching ratio for producing Lyα emissions and the cross sections producing the excited hydrogen in the $n = 2$ and 3 states in process (2). To the best of our knowledge, no experimental or theoretical data concerning these quantities are available despite their importance. Browning *et al* [13] reported that the total charge exchange cross section σ_+ and CH_3^+ formation cross section $\sigma(CH_3^+)$ at 4000 eV (cm) are 4.3×10^{-16} and 2.8×10^{-17} cm^2, respectively, in $He^+ + CH_4$ collisions. The branching ratio of the Lyα emission cross section

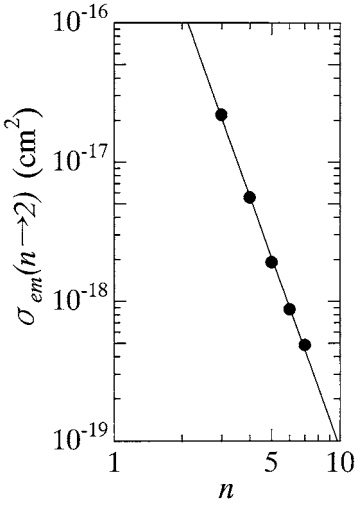

Figure 4. Doubly logarithmic plots of $\sigma_{\rm em}(n \rightarrow 2)$ versus n for Balmer emissions in collisions between He^+ (4000 eV) and CH_4.

$\sigma(\mathrm{Ly}\alpha)$ to the total charge exchange cross section (σ_+) can be determined by the following equation, because the fragment partner of CH_3^+ is the only hydrogen atom with $n = 2$

$$\mathrm{R}(\mathrm{Ly}\alpha) = \frac{\sigma(\mathrm{Ly}\alpha)}{\sigma_{\rm H}(2\mathrm{s}) + \sigma_{\rm H}(2\mathrm{p})} \frac{\sigma(\mathrm{CH}_3^+)}{\sigma_+} \tag{9}$$

where n is the principal quantum number and $\sigma_{\rm H}(n)$ is the hydrogen production cross section in the n state. This branching ratio can be obtained if $\sigma_{\rm H}(2)$ is determined. It was reported by Möhlmann and de Heer [26] that emission cross sections for the hydrogen Balmer series produced by electron impact of CH_4 were given by an empirical formula

$$\sigma_{\rm em}(n \rightarrow 2) = a \cdot n^{-b} \tag{10}$$

where a and b are constants related to the probabilities of predissociation, autoionization and internal conversion of Rydberg states of parent molecule. In addition, Perrin and Aarts [27] proposed a similar formula for hydrogen production cross sections in the n-state,

$$\sigma_{\rm H}(n) = a^* \cdot n^{-b^*} \tag{11}$$

where a^* and b^* are constants. They obtained the value $b^* \sim b - (0.8 \pm 0.3)$ using the average values of branching ratios calculated by Kayrallah [28] for different $(n\ell)$ state-distribution models and assuming a power-law dependence similar to that of $\sigma_{\rm em}(n \rightarrow 2)$. $\sigma_{\rm H}(2)$ is obtained by extrapolating equations (10), (11) and the relation $\sigma_{\rm H}(3) = \sigma_{\rm em}(\mathrm{Ly}\beta) + \sigma_{\rm em}(\mathrm{H}_\alpha)$. Emission cross sections from $\mathrm{H}_\alpha(n = 3)$ to $\mathrm{H}_\varepsilon(n = 7)$at 4000 eV (cm) are shown in figure 4 and table 2. As seen in figure 4 the power-law dependence holds quite well. The values are found to be 3.0×10^{-15} cm^2 and 4.5, respectively, by a least-squares fit. The b value of 4.5 is quite similar to the b value of 4.76 in the case of electron impact on CH_4 as reported by Möhlmann and de Heer [26]. This suggests that the excited state of CH_4 producing H(n) forms a Rydberg-like state converging to the ionic state of CH_4. The a^* and b^* values are calculated to be 2.6×10^{-15} cm^2 and 3.7, respectively, from $\sigma_{\rm H}(3) = \sigma_{\rm em}(\mathrm{Ly}\beta) + \sigma_{\rm em}(\mathrm{H}_\alpha) = 4.4 \times 10^{-17}$ cm^2. The $\sigma_{\rm H}(2)$ $(= \sigma_{\rm H}(2\mathrm{s}) + \sigma_{\rm H}(2\mathrm{p}) = 2.0 \times 10^{-16}$ cm^2) is obtained by equation (10) to yield $R(\mathrm{Ly}\alpha) \sim 2.5 \times 10^{-2}$ at 4000 eV. Then $\sigma_{\rm H}(2)$ and the $\sigma_{\rm H}(3)$ values are displayed as the

Table 2. Emission cross sections of hydrogen Balmer series produced in $He^+ + CH_4$ at 4000 eV (cm).

Species	σ (10^{-18} cm^2)
H_α	21.9
H_β	5.5
H_γ	1.9
H_δ	0.87
H_ε	0.48

cross and the double circle, respectively, in figures 3(*a*) and (*b*). The ratio of $\sigma_H(2)/\sigma_H(2p)$ is evaluated to be 1.2 by comparing $\sigma_H(2)$ with $\sigma(Ly\alpha)$. This value is much larger than in the case of $He^+ + H_2 \rightarrow HeH^+ + H^*(2s \text{ or } 2p)$ as reported by Dhuicq *et al* [29]. They reported that the cross section ratio is around 0.1 at $E_{cm} = 20$ eV and that the scattering angle ranges from 34° to 50°.

4. Conclusion

Emission cross sections for the hydrogen Lyman-α, -β, Balmer-α, -β, C($3s\ ^3P^o_{J'} \rightarrow 2p^2\ ^3P_J$, 165.7 nm), C($2p^3\ ^3D^o_{J'} \rightarrow 2p^2\ ^3P_J$, 156.1 nm) and He($2p\ ^1P_1 \rightarrow 1s^2\ ^1S_0$, 58.4 nm) produced in $He^+ + CH_4$ collision are measured in the energy range from 4 eV (cm) to 4000 eV (cm). The emission cross sections for the hydrogen series have a plateau above 100 eV. The cross section tends to have a larger value with decreasing energy defect at low collision energies. The branching ratio for producing Lyα emission is evaluated as 2.5×10^{-2}.

Acknowledgments

The authors thank Mr T Aoki and Mr N Yamaguchi for their help with the experiments. The authors are also grateful to Professor Bipin Indurkhya and Ms Beryl Nelson for proofreading this manuscript.

References

[1] Miserly M B 1973 *Space Sci. Rev.* **14** 460
[2] Johnson R and Bind M A 1974 *J. Chem. Phys.* **61** 2112
[3] Bryan E L, Freeman E J and Monaco M N 1990 *Phys. Rev.* A **42** 6423
[4] Tsuji M, Cobra K, Boas H and Chino H 1991 *J. Chem. Phys.* **94** 277
[5] Adams N G and Smith D 1976 *J. Phys. B: At. Mol. Phys.* **9** 1439
[6] Huntress W T Jr, Laudenslager J B and Pinizzotto R F Jr 1974 *Int. J. Mass Spectrom. Ion. Proc.* **13** 331
[7] Kim J K and Huntress W T Jr 1975 *Int. J. Mass Spectrom. Ion Proc.* **16** 451
[8] Catham H, Hils D, Robertson R and Gallagher A C 1983 *J. Chem. Phys.* **79** 1301
[9] Bowers M T and Elleman D D 1972 *Chem. Phys. Lett.* **16** 486
[10] Varghese S L, Bissinger G, Joyce J M and Laubert R 1985 *Phys. Rev.* A **31** 2202
[11] Itoh A, Asari M and Fukuzawa F 1980 *J. Phys. Soc. Japan* **48** 943
[12] Koopman D W 1968 *J. Chem. Phys.* **49** 5203
[13] Browning R, Latimer C J and Gilbody H B 1969 *J. Phys. B: At. Mol. Phys.* **2** 534
[14] Brundle C R and Robin M B 1978 *J. Chem. Phys.* **11** 3707
[15] Dillon M A, Wang R G and Spence D 1984 *J. Chem. Phys.* **80** 5581
[16] Wu C Y R and Judge D L 1981 *J. Chem. Phys.* **75** 172
[17] Motohashi K, Soshi H, Ukai M and Tsurubuchi S 1996 *Chem. Phys.* **213** 369
[18] Van Zyl B, Dunn G H, Chamberlain G and Heddle D W O 1980 *Phys. Rev.* **22** 1916

[19] Tsurubuchi S, Miyazaki T and Motohashi K 1996 *J. Phys. B: At. Mol. Opt. Phys.* **29** 1785
[20] Van Zyl B, Jaecks D, Pretzer D and Geballe R 1967 *Phys. Rev.* **158** 29
[21] Pretzer D, Van Zyl B and Geballe R 1963 *Phys. Rev. Lett.* **10** 340
[22] Yamaguchi S, Tsuji M, Obase H, Sekiya H and Nishimura Y 1987 *J. Chem. Phys.* **86** 4952
[23] Massey H S W and Burhop E H S 1952 *Electronic and Ionic Impact Phenomena* (New York: Oxford University Press)
[24] Hasted J B 1960 *Advances in Electronics and Electron Physics* vol 8 (New York: Academic) p 1
[25] Giese C F and Maier W B 1963 *J. Chem. Phys.* **39** 197
[26] Möhlmann G R and de Heer F J 1979 *Chem. Phys.* **40** 157
[27] Perrin J and Arts J F M 1983 *Chem. Phys.* **80** 351
[28] Khayrallah G A 1976 *Phys. Rev.* A **13** 1989
[29] Dhuick D, Jugi B, Benoit C and Sidis V 1998 *J. Chem. Phys.* **109** 512